

Sharp peaks in the conductance of double quantum dot and quantum dot spin-valve systems at high temperatures: A hierarchical quantum master equation approach

S. Wenderoth, J. Bätge, and R. Härtle

Institut für theoretische Physik, Georg-August-Universität Göttingen, D-37077 Göttingen, Germany.

(Dated: September 17, 2021)

We study sharp peaks in the conductance-voltage characteristics of a double quantum dot and a quantum dot spin-valve that are located around zero bias. The peaks share similarities with a Kondo peak but can be clearly distinguished, in particular as they occur at high temperatures. The underlying physical mechanism is a strong current suppression that is quenched in bias-voltage dependent ways by exchange interactions. Our theoretical results are based on the quantum master equation methodology, including the Born-Markov approximation and a numerically exact, hierarchical scheme, which we extend here to the spin-valve case. The comparison of exact and approximate results allows us to reveal the underlying physical mechanisms, the role of first-, second- and beyond-second-order processes and the robustness of the effect.

PACS numbers: 85.35.-p, 73.63.-b, 73.40.Gk

Introduction: Exchange interactions are ubiquitous in quantum many-body physics. They originate from the symmetry of many-body wave functions with respect to the exchange of indistinguishable particles [1, 2]. Imprints of exchange interactions can be found in the energy spectrum of atoms and molecules, scattering cross sections and by the existence of magnetic phases [3, 4]. The description of exchange interactions represents a major challenge. Yet, an exact treatment is crucial. This can be seen, *e.g.*, by the huge effort that is spent in density functional theory to find the correct exchange-correlation functional [5, 6]. Another prominent example is the Kondo effect [7, 8], where the spin of an impurity is screened by itinerant electrons. Here, exchange interactions are attractive and lead to the formation of a bound state, the Kondo singlet. Its binding energy is referred to as the Kondo temperature T_K .

In normal metals like gold, Kondo singlets can lead to an increase of the resistivity at low temperatures [7, 9]. But they can also strongly enhance transport such as, for example, in single-molecule junctions [10–16] or quantum dot devices [17–20], where they establish a direct link between the electrodes. The associated conductivity is the same as the one of a ballistic channel and given by the conductance quantum $G_0 = 2e^2/h \approx 7.75 \cdot 10^{-5} \text{ A/V}$ [19]. The underlying processes need to be coherent such that the effect is found only at low temperatures $T \lesssim T_K$ or, equivalently, small bias voltages where the range of electrons involved in the singlet formation is narrow enough. This leads to very sharp peaks (Kondo peaks) in the corresponding conductance-voltage characteristics at zero bias (cf. the blue line of the schematic conductance map shown in the left panel of Fig. 1).

In this article, we focus on another, complementary transport phenomenon due to exchange interactions. It also leads to sharp peaks in the conductance-voltage characteristics at or near zero bias. Such peaks were reported only recently for double quantum dot (DQD) structures [21] (see middle panel of Fig. 1) and quantum dot spin-valve (SV) setups [22] (see right panel of Fig. 1).

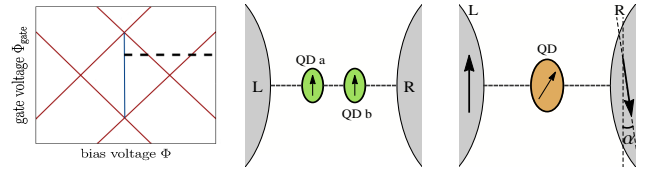


FIG. 1. Left panel: Scheme of a typical conductance map, where the conductance is plotted as a function of both bias and gate voltage. The red diagonals are associated with tunneling through the single-particle levels ϵ_m and $\epsilon_m + U$. The blue line depicts a zero-bias peak. It occurs for gate voltages Φ_{gate} where the impurity or quantum dot system is populated by an odd number of electrons on average. The dashed black line indicates the position of the conductance-voltage characteristics depicted in Fig. 3. Middle panel: Double quantum dot (DQD) where dot a is coupled to the left (L) and dot b to the right electrode (R). Right panel: Quantum dot spin-valve (SV) with non-collinearly polarized electrodes. The angle between the polarization vectors is denoted by α .

Here, we develop a physically intuitive picture, showing that the peak structures can be understood in both systems on the same footing, namely due to orbital and spin exchange processes. We also demonstrate how the peaks can be distinguished from Kondo peaks by experimentally accessible means, in particular their position in asymmetric scenarios [22] and a non-monotonic temperature dependence with a power-law scaling $\sim 1/T^2$ at high temperatures. In addition, we substantially extend previous considerations, which were based on first and second order perturbation theory, by numerically exact results. To this end, we employ the hierarchical quantum master equation technique (HQME) [21, 23] and develop it further to the SV case. We also use approximate Born-Markov results to highlight the robustness of the effect.

Modeling: Both quantum dot systems are naturally described by an impurity part, H_{Imp}^A , a lead part, H_{L+R}^A , and an impurity-lead coupling, $H_{\text{Imp},L+R}^A$ ($A \in \{\text{DQD}, \text{SV}\}$). The DQD structure (middle panel of Fig. 1)

is described by a spinless Anderson impurity model with $H_{\text{Imp}}^{\text{DQD}} = \sum_{m \in \{a,b\}} \epsilon_m d_m^\dagger d_m + U d_a^\dagger d_a d_b^\dagger d_b + (t_{\text{hopp}} d_a^\dagger d_b + h.c.)$, $H_{\text{Imp,L+R}}^{\text{DQD}} = \sum_{m,K,k \in K} \nu_{K,m} t_k c_k^\dagger d_m + h.c.$ and $H_{\text{L+R}}^{\text{DQD}} = \sum_{k \in \{L,R\}} \epsilon_k c_k^\dagger c_k$, where we assume that a magnetic field is used to drive one of the spin species out of the system [24, 25] [26]. It involves two orbitals localized on quantum dots a and b with hopping amplitude t_{hopp} . Double occupation of the orbitals requires an additional charging energy U . The coupling matrix elements $\nu_{K,m}$ and t_k describe the tunneling of an electron from dot m into lead K at energy ϵ_k . The SV system (right panel of Fig. 1) can be modeled by a (spinful) Anderson impurity that is coupled to non-collinearly polarized electrodes with $H_{\text{Imp}}^{\text{SV}} = \sum_{m \in \{\uparrow, \downarrow\}} \epsilon_m d_m^\dagger d_m + U d_\uparrow^\dagger d_\uparrow d_\downarrow^\dagger d_\downarrow$, $H_{\text{L+R}}^{\text{SV}} = \sum_{k \in \{L,R\}, m} \epsilon_{mk} c_{mk}^\dagger c_{mk}$ and $H_{\text{Imp,L+R}}^{\text{SV}} = \sum_{m,m',K,k \in K} \nu_{K,m,m'} t_k c_{m'k}^\dagger d_m + h.c.$. In addition to the DQD case, the coupling matrix elements $\nu_{K,m,m'}$ obtain an additional index, encoding spin-flip processes upon tunneling of an electron with spin m into lead K . The role of the hopping and the spin-flip terms is similar in both systems. They mediate a coherent superposition of the physical degrees of freedom when $\epsilon_{a/\uparrow} \approx \epsilon_{b/\downarrow}$, giving rise to sizeable coherences [21, 27] and, thus, an exchange interaction that quenches the current suppression in a rather narrow range of voltages (see below). Please note that the left and right degrees of freedom of the DQD can be considered as a pseudo-spin degree of freedom that allows a mapping to a spinful Anderson impurity coupled to a single polarized electrode [28]. This mapping, however, does not include a second electrode with a different polarization and/or chemical potential such that, on a formal level, the DQD and SV case are similar but definitely not identical.

Transport theory: We determine the transport properties of the two systems using the HQME technique [21, 23], where we solve the coupled equations of motion

$$\begin{aligned} \partial_t \rho_{j_1 \dots j_\kappa}^{(\kappa)}(t) &= -i \left[H_{\text{Imp}}^A, \rho_{j_1 \dots j_\kappa}^{(\kappa)}(t) \right] - \sum_{\lambda \in \{1 \dots \kappa\}} \omega_{K_\lambda, p_\lambda}^{s_\lambda} \rho_{j_1 \dots j_\kappa}^{(\kappa)}(t) \\ &+ \sum_{\lambda} (-1)^{\kappa-\lambda} \eta_{K_\lambda, p_\lambda}^{s_\lambda} d_{m_\lambda}^{s_\lambda} \rho_{j_1 \dots j_\kappa / j_\lambda}^{(\kappa-1)}(t) \\ &+ \sum_{\lambda} (-1)^\lambda \eta_{K_\lambda, p_\lambda}^{\bar{s}_\lambda, *} \rho_{j_1 \dots j_\kappa / j_\lambda}^{(\kappa-1)}(t) d_{m_\lambda}^{s_\lambda} \\ &- \sum_{j_{\kappa+1}, m'} \Xi_{K_{\kappa+1}, m' m_{\kappa+1}}^{s_{\kappa+1}} \left[d_{m'}^{\bar{s}_{\kappa+1}}, \rho_{j_1 \dots j_\kappa j_{\kappa+1}}^{(\kappa+1)}(t) \right]_{(-1)^{\kappa+1}}, \quad (1) \end{aligned}$$

starting from a product initial state. The density matrix of the impurity enters as $\rho^{(0)}(t) = \rho(t)$. The operators $\rho_{j_1 \dots j_\kappa}^{(\kappa)}(t)$ describe its dynamics due to the coupling to the electrodes. They involve superindices $j = (K, m, s, p)$ with a lead index K , a level index m and an index $s \in \{+, -\}$ corresponding to creation and annihilation processes. The index p is related to a sum-over-poles decomposition of the hybridization and distribution function in the leads. The electrical current $I_K =$

$\sum_{K, mm', p} \Xi_{K, mm'}^+ \text{Tr} \left[\rho_{K, m, +, p}^{(1)}(t) d_{m'} \right] + h.c.$ ($K \in L, R$) is given by the first tier operators. Details of the derivation and explicit expressions for the DQD system can be found in Refs. 21 and 27. Here, we present a generalization of the HQME formalism to the SV case, where the coupling factors $\Xi_{K, mm'}^s$ are given by $\nu_{K, m}^s \nu_{K, m'}^{\bar{s}} / \gamma$ and $(\sum_{\tilde{m}} \nu_{K, \tilde{m}, m}^s \nu_{K, \tilde{m}, m'}^{\bar{s}}) / \gamma$ in the DQD and SV scenario, respectively, and γ is the band width. Note that the HQME (1) are time-local and, therefore, the only method that can be used so far to obtain exact results on the long-lived dynamics in these systems ($t \sim 10^2 - 10^3 / \Gamma$, where Γ denotes the hybridization strength, cf. Ref. [27]).

The hierarchy (1) is infinite, but can be truncated by discarding all terms that belong to a specific tier κ and higher. This represents an approximation of the time evolution operator up to $(\kappa - 1)$ th order in the hybridization strength Γ . Another, systematic truncation scheme is based on assigning each operator $\rho_{j_1 \dots j_\kappa}^{(\kappa)}(t)$ the importance value [21]

$$\left| \prod_{\lambda=1 \dots \kappa} \frac{\eta_{K_\lambda, m_\lambda, p_\lambda}^{s_\lambda} \sum_{m'} \Xi_{K, m_\lambda m'}^{s_\lambda}}{2 \sum_{\lambda'=1 \dots \lambda} \text{Re}[\omega_{K_{\lambda'}, p_{\lambda'}}^{s_{\lambda'}}] \text{Re}[\omega_{K_\lambda, p_\lambda}^{s_\lambda}]} \right|, \quad (2)$$

and including only those terms with a value exceeding a certain threshold. This reduces the numerical complexity to a practical level. Converged or exact results can be obtained for high enough temperatures (typically $T \gtrsim T_K$, see Ref. [29]) while, at lower temperatures, convergence becomes prohibitive. Note that (2) is an extension to the SV case.

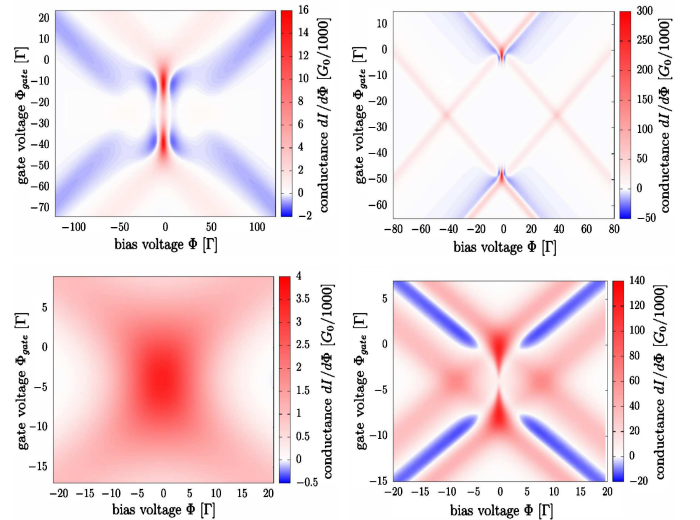


FIG. 2. Conductance maps for symmetric coupling to electrodes, $\Gamma_L = \Gamma_R = \Gamma$. The left and right panels refer to the DQD and SV case, respectively. The upper panels are computed with $U = 50\Gamma$; the lower panels with $U = 8\Gamma$. For even lower U , the maps are similar to the one on the lower left side.

We also present results obtained from the well established Born-Markov master equation (BMME) [30–38]

$$\partial_t \rho(t) = -i [H_{\text{Imp}}^A, \rho(t)] - \int_0^t d\tau \text{tr}_{L+R} \{ [H_{\text{Imp},L+R}^A, [H_{\text{Imp},L+R}^A(\tau), \rho(t) \rho_{L+R}^{\text{equ}}]] \}, \quad (3)$$

where ρ_{L+R}^{equ} denotes the equilibrium density matrix of the leads. The level of approximation is the same as a truncation of (1) at the first tier, including the Markov approximation $\rho(t - \tau) \approx e^{iH_{\text{Imp}}^A \tau} \rho(t) e^{-iH_{\text{Imp}}^A \tau}$.

Results: We consider different parameter regimes of the two systems in order to cover different facets of the phenomenon, in particular slightly higher temperatures in the DQD, $T = 4.5\Gamma$, as compared to the SV case, $T = \Gamma$ (where we use the hybridization strength $\Gamma = 2\pi \max[\Xi_{K,mm}]$ as the unit of energy). The electrodes are modeled in both systems by Lorentzian bands, that is $\sum_{k \in K} |t_k|^2 \delta(\epsilon - \epsilon_{k/mk}) = \gamma / ((\omega - \mu_K)^2 + \gamma^2)$. Note that this choice is not crucial, as we use $\gamma \gtrsim 50\Gamma$ to avoid band edge effects. The bias voltage Φ enters via $\mu_{L/R} = \pm\Phi/2$, the gate voltage via a simple shift of the degenerate single-particle levels, $\epsilon_m = \Phi_{\text{gate}}$. The current is strongly suppressed in the DQD case by a weak coupling between the dots, $t_{\text{hopp}} \approx \Gamma/11$, and in the SV system by almost fully (99%) polarized electrodes and an almost antiparallel configuration of the respective polarization vectors ($\alpha = \pm 0.05\pi$, cf. right panel of Fig. 1).

We introduce the phenomenon by discussing the conductance maps depicted in Fig. 2. The four panels are organized such that the left/right column represents the DQD/SV case, while the top row corresponds to calculations with strong electron-electron interactions, $U = 50\Gamma$, and the bottom row to an intermediate coupling strength, $U = 8\Gamma$. All plots show a prominent peak around zero bias $\Phi \approx 0$ that extends from $\Phi_{\text{gate}} = 0$ to $\Phi_{\text{gate}} = -U$. It has a maximum at a gate voltage $-U/2 < \Phi_{\text{gate}} < 0$ (or $-U < \Phi_{\text{gate}} < -U/2$). The position of the peak is very similar to a ‘Kondo peak’, except that the associated conductance value G is much lower than the conductance quantum, $G \ll G_0$. A technical reason why this can’t be a Kondo resonance is that these calculations are obtained from Born-Markov theory. Similar conductance maps have been obtained using first (cf. Fig. 11 of Ref. 21) and second order perturbation theory (cf. Fig. 7 of Ref. 22). Can we trust the approximate results, in particular as first order processes are strongly suppressed at these voltages and higher order effects dominant?

We verify the validity of previous results by the conductance-voltage characteristics that are shown in Fig. 3. The three lines correspond to the first (red line), second order (blue line) and a fully converged result (black line, which includes terms up to $\mathcal{O}(\Gamma^4)$), where the left panel represents the DQD case with strong and the right panel the SV case with weaker electron-electron interactions. The gate voltage Φ_{gate} is fixed to a value between 0 and $-U/2$ where the conductance peak appears most pronounced (cf. dashed black line in the left panel

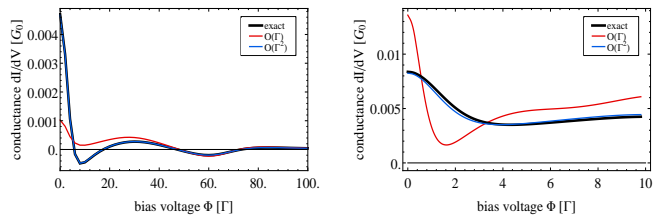


FIG. 3. Conductance-voltage characteristics of the DQD with $U = 50\Gamma$ and $\epsilon_m = -0.3U$ (left panel) and the SV with $U = 8\Gamma$ and $\epsilon_m = -U/4$ (right panel).

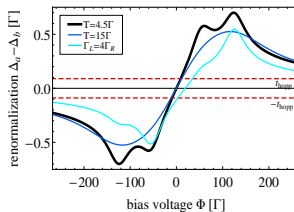


FIG. 4. Difference of the interaction-induced renormalizations $\Delta_a - \Delta_b$ (cf. Eq. (4)). The red dashed lines mark the narrow range of voltages where $|\Delta_a - \Delta_b| < t_{\text{hopp}}$.

of Fig. 1). Overall, the phenomenon turns out to be robust. The second order result is very close to the exact one. Differences between the second order and exact results are significant at lower temperatures (compare SV and DQD case with $T = \Gamma$ and $T = 4.5\Gamma$, respectively).

The origin of the zero bias peak is a strong suppression of the current flow in both systems and interaction-induced renormalization effects [39]. They are included in the principal value terms of the time integrals in (3). In the DQD case, they add to the energy levels $\epsilon_{a/b} \rightarrow \epsilon_{a/b} + \Delta_{a/b}$ and can be estimated by [27, 40]

$$\Delta_{a/b} = \phi_{a/b}(\epsilon_{a/b}, \mu_{L/R}) - \phi_{a/b}(\epsilon_{a/b} + U, \mu_{L/R}), \quad (4)$$

with $\phi_{a/b}(x, \mu) = \frac{\Gamma_{L/R}}{2\pi} \text{Re} \left[\Psi \left(\frac{1}{2} + \frac{i(x-\mu)}{2\pi T} \right) \right]$ and the digamma function $\Psi(x)$. Clearly, if they are neglected, the sharp peak features do not appear (cf. Figs. 11 and 12 of Ref. [21]). For bias voltages $\Phi \neq 0$, the two levels are thus shifted in different directions (see Fig. 4). This is important in situations where $\epsilon_m \ll \mu_{L/R} \ll \epsilon_m + U$, *i.e.* where the dots are populated by one electron. The electron is additionally trapped when $\epsilon_a = \epsilon_b$ such that it can coherently oscillate between the two dots. This trapping is quenched when the levels are disaligned due to the interaction-induced renormalizations $\Delta_{a/b}$. The corresponding range of voltages is rather narrow and, using the uncertainty principle $\Delta E \Delta t = 1/2$ with $\Delta t = \pi/t_{\text{hopp}}$, can be estimated by $|\Delta_a - \Delta_b| \sim t_{\text{hopp}}$ (see Fig. 4). The renormalizations $\Delta_{a/b}$ originate from coherent exchange processes with the electrodes and become effective only in the presence of electron-electron interactions. They translate, *inter alia*, to a coupling between the eigenstates of the DQD $\sim \Delta_a - \Delta_b$ [21]. The corresponding degrees of freedom in the SV case are the spin degrees of freedom, where the interaction-induced coupling quenches the current suppression due to the almost antiparallel polarization of the electrodes. This coupling

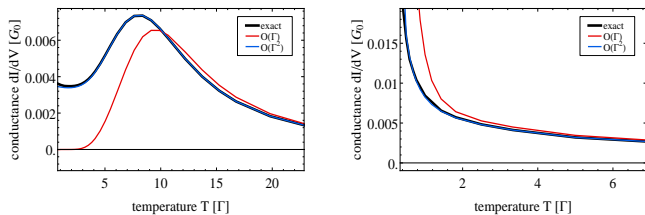


FIG. 5. Zero-bias conductance of the DQD with $U = 50\Gamma$ and $\epsilon_m = -0.3U$ (left panel) and the SV with $U = 8\Gamma$ and $\epsilon_m = -U/4$ (right panel) as a function of temperature T .

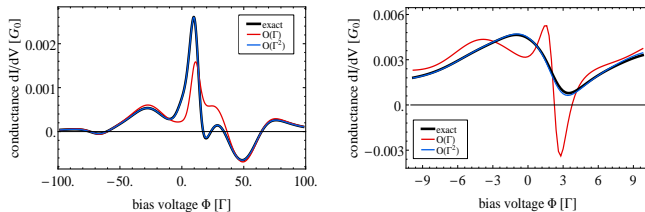


FIG. 6. Conductance-voltage characteristics of the DQD with $U = 50\Gamma$ and $\epsilon_m = -0.3U$ (left panel) and the SV with $U = 8\Gamma$ and $\epsilon_m = -U/4$ (right panel) for an asymmetric coupling to the electrodes, $\Gamma_L = \Gamma = 4\Gamma_R$.

is the exchange interaction mentioned above. Its basics can be understood in terms of first-order arguments but second and beyond-second order effects are apparently important. The coupling interpretation shows that it always leads to an enhanced conductance at low voltages. Otherwise, it can lead to a decrease and even negative differential conductance [40–43] or gate-dependent line shapes [44, 45].

Now, we would like to explain how the sharp peaks can be distinguished from Kondo peaks, since the unitary limit $G = G_0$ is not accessible in all experimental setups. Thus, evidence is typically derived from the temperature dependence of the conductance, which we show in Fig. 5. The DQD case (left panel) shows a non-monotonic peak structure at intermediate temperatures that is followed by a power-law decay $\sim 1/T^2$ (which converts to a well-known $1/T$ scaling when thermal broadening becomes dominant; see lower left panel of Fig. 2). The same scaling is also observed in the SV case (right panel). This behavior results from the non-monotonic temperature dependence of the interaction-induced renormalizations, that is $\Delta_a - \Delta_b \xrightarrow{T \rightarrow 0} u + vT^2$ and $\Delta_a - \Delta_b \xrightarrow{T \rightarrow \infty} \Phi/T^2$, including a peak at intermediate temperatures which is also seen in the conductance-temperature characteristics. For weaker U , it is shifted to lower temperatures and, therefore, not visible in the weak coupling SV case (right panel of Fig. 5). This analytic finding is in clear contrast to a Kondo peak, where we expect a monotonic decay and a different scaling behavior [8, 46]. Note that the conductance maxima (red spots in the upper panels of Fig. 2) also show an interesting temperature dependence.

In the DQD case with $U = 50\Gamma$, they are shifted towards the charge-symmetric point when increasing temperature (data not shown). This is in clear contrast to Kondo peaks, but we also observe the opposite behavior such that a clear distinction is not possible.

The cleanest distinction can be made in systems where the coupling to the electrodes is asymmetric, $\Gamma_L \neq \Gamma_R$. The conductance-voltage characteristics of such scenarios are shown in Fig. 6. In contrast to symmetric coupling, the sharp conductance peaks no longer appear at zero but at non-zero bias voltages [22]. This can be readily seen by the dependence of the interaction-induced renormalizations (4) on the hybridization strengths, $\Delta_{a/b} \sim \Gamma_{L/R}$ (see turquoise line in Fig. 4). For $\Gamma_L > \Gamma_R$, the root of the difference $\Delta_a - \Delta_b$ is shifted from $\Phi = 0$ to a non-zero, positive bias voltage, which corresponds to the peak position in the conductance-voltage characteristics. The maximal shift is $\Phi = \pm(2\epsilon_0 + U)$, which can be derived from the condition $\Delta_{a/b}(\Phi) = 0$ in the limit $\Gamma_{L/R} \rightarrow 0$. The peak structure gets suppressed as $\Gamma_{L/R} \rightarrow 0$ and vanishes faster including higher order effects (cf. right panel of Fig. 6). Note that a similar behavior emerges for detuned levels, where $\epsilon_a - \epsilon_b = 0.4\Gamma$ corresponds to $\Gamma_L = \Gamma = 4\Gamma_R$.

Conclusions: We studied sharp peaks in the conductance-voltage characteristics of double quantum dot and spin-valve systems with (quasi-)degenerate single-particle levels. We showed that the peaks can be understood in both systems on the same footing, namely in terms of exchange interactions that quench a strong, inherent current suppression. In symmetric systems, the peaks are located at the same voltages as Kondo peaks but can be clearly distinguished by their $1/T^2$, sometimes even non-monotonic temperature dependence. In asymmetric or detuned systems, the distinction is even easier, because the peaks occur at non-zero bias voltages and one bias polarity [22]. Our analysis is based on the hierarchical quantum master equation technique, which allows us to compare first and second order results with numerically converged, exact results. Thus, we were able to demonstrate the robustness of the phenomenon and the role of higher order effects. We also used results derived from Born-Markov theory, demonstrating the importance of principal value terms in the presence of quasidegenerate energy levels. Our study underlines the importance of an exact description of exchange interactions. This can be even more relevant in transport through more complex systems such as, for example, multi-dot systems or molecular junctions where quasidegeneracies are even more important. In contrast to Kondo peaks, the peaks described here are more robust with respect to bias voltage and temperature. This is beneficial from both an experimental and a technological point of view.

Acknowledgement: We thank A.J. Millis, J. Okamoto, M. Wegewijs, J. König, P. Wang, K. Schönhammer and S. Kehrein for helpful comments and discussions. RH is supported by Deutsche Forschungsgemeinschaft (DFG) under grant No. HA 7380/1-1.

-
- [1] W. Heisenberg, *Z. Physik* **38**, 411 (1926).
- [2] P. A. M. Dirac, *Proceedings of the Royal Society of London. Series A, Containing Papers of a Mathematical and Physical Character* **112**, 661 (1926).
- [3] J. B. Goodenough, *Magnetism and the Chemical Bond* (Interscience Publishers, New York, 1966).
- [4] R. W. White, *Quantum Theory of Magnetism: Magnetic Properties of Materials* (Springer, Berlin, 2007).
- [5] W. Kohn and L. J. Sham, *Phys. Rev.* **140**, A1133 (1965).
- [6] E. Engel and R. M. Dreizler, *Density Functional Theory* (Springer, Berlin, 2011).
- [7] J. Kondo, *Prog. Theor. Phys.* **32**, 37 (1964).
- [8] A. C. Hewson, *The Kondo problem to Heavy Fermions* (Cambridge University Press, Cambridge, 1993).
- [9] W. J. de Haas, J. de Boer, and G. J. van den Berg, *Physica (Utrecht)* **1**, 1115 (1934).
- [10] W. Liang, M. Shores, M. Bockrath, J. Long, and H. Park, *Nature (London)* **417**, 725 (2002).
- [11] A. N. Pasupathy, R. C. Bialczak, J. Martinek, J. E. Grose, L. A. K. Donev, P. L. McEuen, and D. C. Ralph, *Science* **306**, 86 (2004).
- [12] L. H. Yu, Z. K. Keane, J. W. Ciszek, L. Cheng, J. M. Tour, T. Baruah, M. R. Pederson, and D. Natelson, *Phys. Rev. Lett.* **95**, 256803 (2005).
- [13] E. A. Osorio, K. O'Neill, M. Wegewijs, N. Stuhr-Hansen, J. Paaske, T. Bjørnholm, and H. S. J. van der Zant, *Nano Lett.* **7**, 3336 (2007).
- [14] A. Mugarza, C. Krull, R. Robles, S. Stepanow, G. Ceballos, and P. Gambardella, *Nature Communications* **8**, 490 (2011).
- [15] D. Rakhmievitch, R. Korytar, A. Bagrets, F. Evers, and O. Tal, *Phys. Rev. Lett.* **113**, 236603 (2014).
- [16] S. Wagner, F. Kisslinger, S. Ballmann, F. Schramm, R. Chandrasekar, R. Bodenstern, O. Fuhr, D. Secker, K. Fink, M. Ruben, and H. B. Weber, *Nat. Nanotechnology* **8**, 575 (2013).
- [17] D. Goldhaber-Gordon, H. Shtrikman, D. Mahalu, D. Abusch-Magder, U. Meirav, and M. A. Kastner, *Nature* **391**, 156 (1998).
- [18] S. M. Cronenwett, T. H. Oosterkamp, and L. P. Kouwenhoven, *Science* **281**, 540 (1998).
- [19] W. G. van der Wiel, S. De Franceschi, J. M. Elzerman, T. Fujisawa, S. Tarucha, and L. P. Kouwenhoven, *Science* **282**, 2105 (2000).
- [20] H. Jeong, A. M. Chang, and M. R. Melloch, *Science* **293**, 2221 (2001).
- [21] R. Härtle, G. Cohen, D. R. Reichman, and A. J. Millis, *Phys. Rev. B* **88**, 235426 (2013).
- [22] M. Hell, B. Sothmann, M. Leijnse, M. R. Wegewijs, and J. König, *Phys. Rev. B* **91**, 195404 (2015).
- [23] J. Jin, X. Zheng, and Y. Yan, *J. Chem. Phys.* **128**, 234703 (2008).
- [24] W. G. van der Wiel, S. De Franceschi, J. M. Elzerman, T. Fujisawa, S. Tarucha, and L. P. Kouwenhoven, *Rev. Mod. Phys.* **75**, 1 (2002).
- [25] A. J. Keller, S. Amasha, I. Weymann, C. P. Moca, I. G. Rau, J. A. Katine, H. Shtrikman, G. Zarand, and D. Goldhaber-Gordon, *Nat. Phys.* **10**, 145 (2014).
- [26] Using units where the elementary charge $e = 1$, $\hbar = 1$ and the Boltzmann constant $k_B = 1$.
- [27] R. Härtle and A. J. Millis, *Phys. Rev. B* **90**, 245426 (2014).
- [28] V. Kashcheyevs, A. Schiller, A. Aharony, and O. Entin-Wohlman, *Phys. Rev. B* **75**, 115313 (2007).
- [29] R. Härtle, G. Cohen, D. R. Reichman, and A. J. Millis, *Phys. Rev. B* **92**, 085430 (2015).
- [30] V. May, *Phys. Rev. B* **66**, 245411 (2002).
- [31] A. Mitra, I. Aleiner, and A. J. Millis, *Phys. Rev. B* **69**, 245302 (2004).
- [32] J. Lehmann, S. Kohler, V. May, and P. Hänggi, *J. Chem. Phys.* **121**, 2278 (2004).
- [33] U. Harbola, M. Esposito, and S. Mukamel, *Phys. Rev. B* **74**, 235309 (2006).
- [34] J. Koch, M. Semmelhack, F. von Oppen, and A. Nitzan, *Phys. Rev. B* **73**, 155306 (2006).
- [35] L. Siddiqui, A. W. Ghosh, and S. Datta, *Phys. Rev. B* **76**, 085433 (2007).
- [36] C. Timm, *Phys. Rev. B* **77**, 195416 (2008).
- [37] R. Härtle, C. Benesch, and M. Thoss, *Phys. Rev. Lett.* **102**, 146801 (2009).
- [38] R. Härtle and M. Thoss, *Phys. Rev. B* **83**, 115414 (2011).
- [39] J. König and J. Martinek, *Phys. Rev. Lett.* **90**, 166602 (2003).
- [40] B. Wunsch, M. Braun, J. König, and D. Pfannkuche, *Phys. Rev. B* **72**, 205319 (2005).
- [41] J. N. Pedersen, B. Lassen, A. Wacker, and M. H. Hettler, *Phys. Rev. B* **75**, 235314 (2007).
- [42] P. Trocha, I. Weymann, and J. Barnas, *Phys. Rev. B* **80**, 165333 (2009).
- [43] A. Donarini, G. Begemann, and M. Grifoni, *Phys. Rev. B* **82**, 125451 (2010).
- [44] J. V. Holm, H. I. Jorgensen, K. Grove-Rasmussen, J. Paaske, K. Flensberg, and P. E. Lindelof, *Phys. Rev. B* **77**, 161406 (2008).
- [45] G. Begemann, S. Koller, M. Grifoni, and J. Paaske, *Phys. Rev. B* **82**, 045316 (2010).
- [46] D. Goldhaber-Gordon, J. Göres, M. A. Kastner, H. Shtrikman, D. Mahalu, and U. Meirav, *Phys. Rev. Lett.* **81**, 5225 (1998).